Electrochemical Detection of PFAS Contaminants Across Environmental and Pharmaceutical Matrices:Sensing Mechanisms, Nanomaterial Platforms, Biological Monitoring, and Regulatory Convergence

Jyoti Rani[1], Alka Sharma[1*], Nisha Chaudhary[1], Saurabh Saklani[1*], Harbhajan Singh[2], Vishal Rihal[2]

[1]Assitant Professor, School of Pharmacy and Emerging Sciences, Baddi University of Emerging Sciences & Technology, Baddi Makhnumajra- 173205, H.P. India.

[2]Research Scholar, School of Pharmacy and Emerging Sciences, Baddi University of Emerging Sciences &Technology, Baddi Makhnumajra- 173205, H.P. India.

Abstract

PFAS are a class of over 14,000 synthetic compounds characterized by a stable carbon-fluorine bond that confers resistance to thermal and biological degradation, resulting in common contamination of various aquatic matrices at concentrations ranging from sub-parts per trillion to parts per billion. Demand for directly deployable sensitive quantification methods has been spurred by increasingly stringent regulatory responses such as the U.S. Environmental Protection Agency (EPA) proposed maximum contaminant levels of 4 ppt for PFOA and PFOS in 2024 under its third Fourth Unregulated Contaminant Monitoring Rule and sub-parametric values recommended by the EU Drinking Water Directive. Conventional liquid chromatography-tandem mass spectrometry provides the required sensitivity but is still limited by centralized infrastructure and slow sample preparation that prevents point-of-care or real-time surveillance. Another critically understudied dimension includes pharmaceutical matrices, where PFAS can act as formulation excipients or derive from the synthesis of fluorinated active pharmaceutical ingredients and pharmacokinetically interfere with albumin binding and hepatic CYP450 activity in exposed populations. The current review summarized the existing electrochemical sensing strategies, including molecularly imprinted polymers, aptasensors, and CRISPR-Cas12a biosensors, and state-of-the-art electrode structures, including metal-organic frameworks, MXenes, and covalent triazine frameworks, for targeting PFAS in environmental and biological matrices. While some of these can be implemented analytically with detection below 1 ppt, critical benchmarking using regulatory thresholds reveals that 10% of sensor studies validate their performance in non-spiked field or clinical matrices. This highlights the need for multi-analyte array development to allow standardized sensor validation frameworks across environmental and pharmaceutical quality monitoring.

Keywords: PFAS; electrochemical sensor; molecularly imprinted polymer; aptasensor; CRISPR-Cas12a; environmental water monitoring; pharmaceutical matrix; biological biomonitoring; adsorptive stripping voltammetry.

How to cite this article: Rani J, Sharma A, Chaudhary N, Saklani S, Singh H, Rihal V. Electrochemical Detection of PFAS Contaminants Across Environmental and Pharmaceutical Matrices: Sensing Mechanisms, Nanomaterial Platforms, Biological Monitoring, and Regulatory Convergence. Int J Drug Deliv Technol. 2026;16(72s): 1771-1790. DOI: 10.25258/ijddt.16.72s.196

1. Introduction: PFAS as a Global Water and Pharmaceutical Crisis

PFASs are chemically diverse substances sharing the common feature of the presence of one or more C–F bonds, with a bond dissociation energy (BDE) of ~544 kJ/mol, generally considered one of the highest BDE values in organic chemistry. This thermodynamic stability, along with the combined lipophobic and hydrophobic nature of perfluorinated alkyl chains, makes PFAS nearly impervious to thermal degradation, oxidative attack, and microbial metabolism on long-term timescales [1]. These compounds were originally developed in the 1940s for industrial, military, and consumer applications and are found in Arctic ice cores, deep-sea sediments, remote wildlife blood, and drinking water supplies without a proximal industrial source because of their atmospheric transport and hydrological mobility properties that also show up as low soil sorption coefficients for short-chain variants. High albumin binding affinity and enterohepatic recirculation contribute to serum half-lives in humans of 3-8 and 5.4 years for perfluorooctanoic acid (PFOA) and perfluorooctane sulfonate (PFOS), the most well-characterized compounds in the long-chain carboxylate and sulfonate subclasses [2]. PFOS levels in groundwater routinely exceed Mrds at aqueous film-forming foam sites at military airfields across North America, Europe, and Australia. Short-chain substitute agents, e.g., perfluorobutanoic acid, butane sulfonate, and

hexafluoropropylene oxide dimer acid, further span control limitations through enhanced aqueous mobility and accumulated indication of analogous toxicological effectiveness at ecologically critical concentrations [3].

There is a substantial health burden that supports regulatory action. In 2023, the International Agency for Research on Cancer classified PFOA as a Group 1 human carcinogen based on sufficient epidemiological evidence of kidney cancer in occupationally and environmentally exposed cohorts and PFOS as a Group 2B carcinogen. Mechanistic pathways include disruption of lipid and bile acid homeostasis via peroxisome proliferator-activated receptor-alpha agonism and competitive displacement of thyroid hormones from transthyretin and thyroxine-binding globulin, impairing metabolic and neurodevelopmental regulation, suppression of vaccine-induced antibody responses at serum concentrations documented in some communities poisoned with these chemicals [4]. Large international prospective cohort studies provide evidence of an association between prenatal exposure, reduced birth weight, delayed onset of puberty, and neurodevelopmental sequelae. Ecotoxicological bioaccumulation amplifies these effects through aquatic food webs to tissue concentrations in piscivorous seabirds and marine mammals' orders of magnitude above the surrounding water, with reproductive/developmental toxicity confirmed at environmentally relevant concentrations. This toxicological evidence caused an unprecedented regulatory response. In April 2024, the U.S. Environmental Protection Agency published National Primary Drinking Water Regulations with maximum contamination levels of 4 ppt for individual PFOA and PFOS, 250 times below previous advisory levels; and a health index framework for hexafluoropropylene oxide dimer acid, perfluorononanoic acid, perfluorohexane sulfonate, and perfluorobutane sulfonate, with compliance no later than 2029 [5]. In parallel, the relayed Drinking Water Directive of the European Union proposed a parametric sum of 0.10 µg/L for 20 specific PFAS and 0.50 µg/L with respect to all detectable PFAS that require simultaneous multi-analyte quantification among EU member states until 2026. These thresholds are close to what current reference methods can quantify, making this analytical challenge as difficult as the regulatory challenge [6].

Liquid chromatography-tandem mass spectrometry (LC-MS/MS) by EPA Methods 533 and 537.1 achieves instrument detection limits (ILDs) of 0.1-1 ppt for >40 analytes and is the regulatory reference standard, but high instrumentation cost, requirement for skilled operators, complexity of solid phase extraction methods that leave scope for contamination via PFAS-containing lab materials in either sample preparation or pre-concentration, plus a sample to results turnaround time of " Enzyme-linked immunosorbent assay kits are more accessible in field environments, but they exhibit cross-reactivity among structurally diverse PFAS classes, cannot differentiate between long-chain and short-chain congeners, and cannot provide compound-specific information needed for hazard index calculations. There is, therefore, a growing and urgent need for PFAS measurement at point of care in human biological matrices on either system [7]. A component of PFAS pollution that has not yet received sufficient attention by environmental monitoring strategies is the overlap with pharmaceutical science, which has led to three functionally distinct monitoring needs. PFAS are used as structural excipients in metered-dose inhaler valve components, dry powder inhaler capsule shells, and transdermal patch membranes to modulate or impair drug particle properties on surface-altered solid surfaces and to form fluoropolymer-laminated, emulsion-formed flexible polyurethane foam lining of manufacturing equipment with cleaning validation studies documenting quantifiable PFAS transfer to aqueous drug product batches under operational conditions [8]. A significant but poorly characterized point source of pharmaceutical synthesis. Effluents (output) from the Hyderabad manufacturing cluster contain up to 4200 ppt PFOA and 890 ppt PFOS, well above EPA MCLs, in wastewater (input) entering treatment systems with no removal requirements. Most jurisdictions lack specific pharmaceutical sector-wide limits on PFC discharges. Importantly, concentrations of circulating PFAS observed in exposed populations pharmacokinetically interact with co-administered therapeutics like PFOA and PFOS, competitively displacing warfarin from Sudlow Site II on albumin (micromolar disassociation constants); inhibit CYP3A4, CYP2C9, and UGT1A1 in hepatic microsome systems at 10-100 µM; and displace thyroxine from thyroxine-binding globulin, directly complicating dose titration of levothyroxine, the most prescribed drug globally in exposed patients. These interactions necessitate PFAS quantification in serum, plasma, urine and other biological matrices at sensitivity and throughput regimes that avoid centralised laboratory infrastructure [9,10].

Electrochemical sensing meets this need for convergent environmental and pharmaceutical monitoring with miniaturizable, field-deployable instrumentation compatible with sub-part-per-trillion detection without the use of mass spectrometric infrastructure. Indirect transduction approaches (for analytes that lack oxidizable or reducible functional groups through the usable aqueous potential window) employ surface adsorption, bioreceptor-mediated recognition, and interfacial impedance modulation [11]. The source-

to-surface and groundwater-to-human biology exposure pathways of PFAS are schematically illustrated in the continuum diagram of **Figure 1**; each node in this pathway requires a unique but technologically compatible sensing solution, a critical and comprehensive survey on the current status of electrochemical PFAS sensing across this continuum, including molecularly imprinted polymer sensors, aptasensors, CRISPR-Cas12a-coupled biosensors, and advanced electrode architectures such as metal–organic frameworks (MOFs), MXenes, covalent triazine frameworks (CTFs), and bismuth film platforms; benchmarking reported detection limits against EPA- and EU-compliant thresholds; and performance metrics in pharmaceutical effluent and serum-dried blood spot-urinary matrices before charting the translational gaps pertaining to field validation, multi-analyte array design, and AI-assisted chemo metric interpretation that must be addressed if electrochemical sensors are to fulfill their regulatory or clinical potential [12,13].

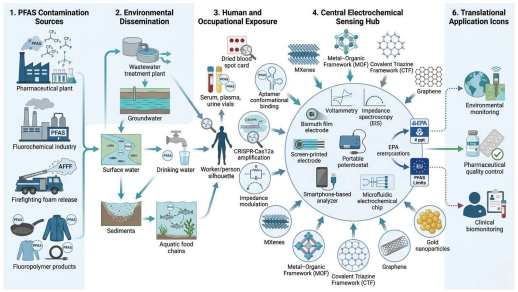

Figure 1. Schematic representation of PFAS contamination pathways from industrial, pharmaceutical sources to environmental dissemination and human exposure. The figure also depicts integrated electrochemical sensing workflows for PFAS monitoring in environmental and biological matrices.

2. Electrochemical characteristics of PFAS and the principle of indirect determination

The electrochemistry of PFAS is fundamentally different from all other classes of relevant environmental contaminants, and a fundamental comprehension of this difference is required for the discussion of sensor architectures in the following sections. These sub-sections sequentially define the electronic bases of PFAS electroinertness, outline the indirect sensing approaches required by this inertness, and analyze the signal transduction mechanisms required to translate these strategies into regulatory-testing-competitive analytical capabilities.

2.1 Electroinertness of PFAS Molecules and Basic Detection Method

The intrinsic electroanalytical challenge of PFAS detection is the electronic structure of this highly stable perfluorinated carbon chain. In comparison, none of these characteristics occur in perfluoroalkyl substances, whereas heavy metals, which can be deposited by anodic stripping; phenolic endocrine disruptors oxygenated at carbon electrodes; or nitroaromatic compounds reducible at moderate negative potentials all have accessible π-electron systems, oxidizable heteroatom functional groups, and readily reducible groups within the aqueous electrochemical window of ca. −1.2 to +1.8 V versus Ag/AgCl on carbon substrates [14]. The HOMO-LUMO gaps for PFOA and PFOS are 9.41 and 9.18 eV, respectively, and are among the largest reported for environmental chemicals by far, as shown by B3LYP/6–311+G** density functional theory calculations, due to the electron-withdrawing perfluoroalkyl chain that makes the carboxylate and sulfonate head groups very resistant to direct faradaic processes (**Figure 2**). Such electronic passivity requires a fundamentally different detection paradigm. Electroanalysis is not based on direct oxidation or reduction but on adsorptive preconcentration and relayed signal transduction via competitive displacement of a redox-active reporter, interfacial impedance reconfiguration upon receptor-PFAS binding, or bioreceptor-coupled amplification cascades [15,16].

Adsorptive stripping voltammetry takes advantage of the amphiphilicity of PFASs. The hydrophobic interaction between the perfluorinated tail and the electrode surface, together with the electrostatic attraction between the anionic polar head group and the positive surface sites, results in the spontaneous accumulation at the interface [17]. In the traditional two-step system, PFAS accumulate ~30-180 s at open circuit before differential pulse or square wave voltammetry measures competitive displacement of a pre-adsorbed redox probe, ferricyanide or hexaammineruthenium, or double layer capacitance changes due to the built-up amphiphilic monolayer. Molecular dynamics simulations and sum-frequency generation spectroscopy both show that PFAS preferentially orient at the electrode-water interface, with the fluorinated tail focused toward hydrophobic regions of the electrode and the ionic solvent-exposed head group facing into the bulk of water [18]. The free energy of adsorption for PFOS onto graphene is calculated to be −42.3 kJ/mol with an increasing affinity with increasing chain length due to higher surface contact area and steric conformationmechanistic evidence corroborated by this correlation at high sensitivity, allowing detection limits in adsorptive (cus) platforms across literature [19,20]. Electrodeposited bismuth film electrodes can chelate PFAS more efficiently than glassy carbon or carbon paste as shown by X-ray photoelectron spectroscopy (Bi–F binding energy of 686.2 eV after PFOS contact), through bismuth fluoride coordination at oxide surface layer and achieve detection limits of 1–5 ppt for PFOS and

PFOA under conditions optimized for accumulation potential, electrolyte pH, and ionic strength, but their performance is inhibited in solution with competing surfactants and natural organic matter. Less toxic alternatives are antimony film electrodes, which show similar analytical performance and lower sensitivity to the speciation changes with different ionic compositions of the samples [21].

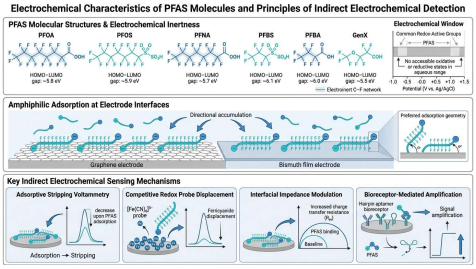

Figure 2. Representative molecular structures and electrochemical characteristics of major subclasses of PFAS depicting the electroinert nature of perfluorinated carbon chains. The reason for the preference for indirect electrochemical detection strategies is explained by HOMO–LUMO gap analysis and interfacial adsorption behaviour.

2.2 Structures for Indirect Signal Transduction and Amplification

Competitive displacement strategies (CDS) form a complementary mechanism to conventional indirect detection approaches, exploiting the high binding affinity of PFAS for hydrophobic electrode surfaces or functionalized receptor layers and quantitative competition-based displacement of pre-adsorbed redox-active reporters proportional to analyte concentrations. developed an electroactive reporter to detect PFAS binding to self-assembled alkyl-thiol monolayers on gold electrodes, which was converted into a molecularly imprinted polymer sensor format where PFAS-induced conformational changes of the crosslinked polymer matrix modulate charge transport and redox probe access to the electrode surface [22,23]. Two-stage architectures based on fluorophilic sorbent preconcentration and electrochemical detection on a single platform achieve 100–1000-fold enrichment factors to concentrate sub-part-per-trillion environmental concentrations into the measurable range of indirect transduction without reliance on solid-phase extraction or mass spectrometric equipment. Main sensing strategies are compared schematically in **Figure 3.**

Low intrinsic signal of indirect electrochemistry requires multi-level amplification to reach LC-MS/MS biodetection limits. Nanostructuring by deposition/functionalization of gold nanoparticles, carbon nanotubes, or graphene oxide increases the electroactive surface area by 10-50-fold together with the preconcentration capacity and signal magnitude. Fluorophilic surface coatings of bifunctional nanoparticles will enable integration of both recognition and amplification into a single nanoscale construct with electroactive cores that transduce signals for the accumulation of PFAS [24]. The attomolar detection limits of PFOA using horseradish peroxidase-labeled secondary aptamers for enzymatic signal amplification in sandwich bioassay formats. Electrochemiluminescence transduction (via luminescence from excited-state electrochemical intermediates) provides 10–100-fold sensitivity gains over state-of-the-art differential pulse voltammetry-based approaches. Combined with CRISPR-based nucleic acid amplification, to our knowledge this represents the lowest detection limits reported for such an electrochemical PFAS platform. Collectively, these amplification architectures overcome the sensitivity barrier imposed by the electronic inactivity of perfluorinated analytes. The possibilities at both mechanistic and instrumental levels for the advanced sensor platforms discussed in the following sections[25].

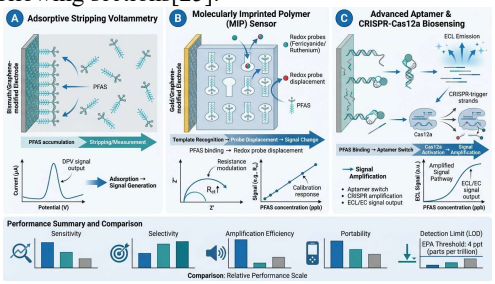

Figure 3. Comparative illustration of major indirect electrochemical sensing mechanisms for PFAS detection including adsorptive stripping voltammetry, molecularly imprinted polymer sensing, and aptamer-based electrochemiluminescence biosensing. Representative signal transduction pathways and analytical response trends of PFOS and PFOA are also summarised.

3. Electrochemical Sensors Based on Molecularly Imprinted Polymers

Molecularly imprinted polymers are a specific synthetic receptor approach specifically suited for PFAS electrochemical detection, solving the dual challenges of few natural biological receptors with high binding affinity to perfluorinated compounds and the low immunogenicity of fluorinated analytes, which limits the development of antibody-based immunoassay. Rational MIP architectures selective for PFAS, their integration with emerging high-performance electrode nanomaterials, and translation toward multi-analyte systems are addressed in the next subsection.

3.1 Template selection, electropolymerized MIP films and functional monomer design

An effective PFAS MIP must be effectively developed by taking advantage of the dual chemical nature of perfluoroalkyl analytes where

ionic interactions between cationic monomers, primarily 2-(methacryloyloxy)ethyl trimethylammonium chloride, and carboxylate or sulfonate head groups are enhanced by hydrophobic interactions between the fluorinated chain and the polymer matrix during cross-linking [26]. Using NOESY NMR-determined interaction geometries for the PFOA template and DFT-calculated binding energies (-8.4, -9.1, & -7.6 kcal/mol for PFOA), acrylamide, itaconic acid and 4-vinylpyridine are identified as functionally optimal monomers. The incorporation of fluorinated functional monomers like 2-(trifluoromethyl)acrylic acid makes the cavity walls fluorophilic due to C-F...H-C and C-F...C-F interactions, which significantly improves the recognition of short-chain PFAS in the separation, compared to conventional hydrophobic monomers, where the weaker driving forces from noncovalent bonding with standard monomers limit the molecular sensitivity of short-chain PFAS compared to long ones [27]. The need for blank subtraction protocols for template leaching during synthesis, as well as contamination of laboratory plasticware is discussed. The use of shorter chain PFAS as synthetic proxies in structural analogue templates reduces contamination risk without loss of geometric cavity complementarity, although explicit validation of cross-reactivity profiles prior to supervision in regulatory monitoring contexts is mandatory [28]. Their clinical commonality challenged their ability to cause greater MIP detection on the surface of the electrode in a single step, which allows for simultaneous polymer formation and molecularly imprinted electrode modification without any intermediate step. The prior research showed that densely packed amine- and catechol-functionalized surfaces provide complementarity in hydrogen bonding and π-Electrochemical impedance spectroscopy detects PFOA at 1.5 ppt using polydopamine molecularly imprinted polymers on glassy carbon electrodes modified with gold nanoparticles. stacking interactions to optimize interactions with the carboxylate head group. 0.8 parts per trillion detection limits by differential pulse voltammetry were obtained for polyaniline molecularly imprinted polymer films on carbon nanotube-modified screen-printed electrodes prepared by cyclic voltammetric electro polymerization using perfluorooctanesulfonate (PFOS) as the template, with selectivity coefficients of 8.4-fold preference for PFOS over perfluorooctanoic acid (PFOA) at equal concentrations [29]. Electro polymerization of orthophenylene diamine on reduced graphene oxide modified glassy carbon electrodes results in dense, highly crosslinked films with narrow cavity dimensions that are suitable for differentiating PFAS based on head group chemistry and for the detection of both PFOS (1.2 ppt) and PFOA (2.0 ppt) with recoveries of 96–104% in spiked river water achieving performance equivalent to EPA MCL thresholds under controlled matrix conditions (**Figure 4).**The critical parameters determining the sensitivity of electropolymerized MIP performance: deposition potential waveform; template-to-monomer molar ratio and the protocol for extracting the template, usually 0.5–1.0 M NaOH in methanol–water, an incomplete extraction (proven to be a major factor for lower sensitivity), needs explicit indication as background signal stabilises after successive extractions until blank absorbance no longer dips [30,31].

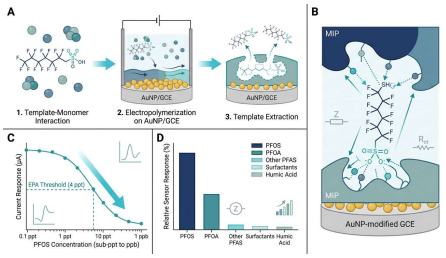

Figure 4. Schematic representation of molecularly imprinted polymer preparation, selective PFAS recognition, and electrochemical sensing performance on AuNP/GCE platforms. The calibration behaviour and selectivity towards PFOS over structurally related interferents are also shown.

3.2 Short-chain Detection and Multi-PFAS Array Platforms Enhanced by Nanoparticles

Low dimensional nanostructures like gold nanoparticles, carbon nanofibers and magnetic iron oxide particles embedded within or underneath MIP films, overcome the limitation of electron transport in thick polymer matrices and at the same time improve the preconcentration capacity. Polyaniline M IP composites with carbon nanofiber-enhanced electron transport pathways connecting analyte-binding cavities to the current collector are sufficient for PFOS detection as low as 0.6 ppt; magnetic nanoparticle-incorporated composites that concentrate 100 mL sample volumes directly onto the sensor surface provide both this enrichment factor and sub-part-per-trillion detection capability in complex environmental matrices without solid-phase extraction infrastructure [32,33]. However, their clinical commonality challenged their ability to cause greater MIP detection due to: reduced hydrophobic attachment in a smaller cavity; a reduced molecular footprint lowering occupancy and thermodynamic goodness-of-fit resulting in less tendency for surface accumulation; and high aqueous solubility within suggested vapour pressures. Published MIP sensors for these analytes have detection limits in the range of 5-50 ppt and are therefore unsuitable for direct compliance monitoring without preconcentration [34]. Cyclodextrin-based co-recognition elements embedded within the polymer

matrix provide further inclusion complex formation, enhancing short-chain carboxylic acids sensitivity by two-to-four fold in proof-of-concept configurations. Dual-template imprinting in one polymer matrix enabled CPE-based simultaneous detection using electrochemical impedance spectroscopy at 1.8 and 1.5 ppt, respectively, for multi-PFAS (PFOA and PFOS) needed for EPA Hazard Index compliance and EU sum-parametric verification [35]. Spatially distinct MIP-modified electrodes within an array (each electrode imprinted with a unique PFAS template on the same printed substrate), interfaced to principal component analysis and partial least squares regression extend simultaneous quantification from two to four or six analytes but can provide additional internal consistency verification using correlated response patternsan essential countermeasure that protects against false-positives generated by non-specific matrix interferences that identifies research priorities for multi-analyte sensors in the final section [36].

4. Electrochemical Aptamer-Based Biosensors and CRISPR-Coupled Platforms

While molecularly imprinted polymers establish PFAS recognition by means of synthetic cavity complementarity, aptamer-based platforms utilize nucleic acid folding thermodynamics to yield bioreceptors with dissociation constants in the low nanomolar range - a binding affinity window that with electrocatalytic transduction and nuclease-based amplification cascades, is realized to extend detection limits one to two orders of magnitude below EPA MCL levels. In the following subsections, we explore SELEX-derived aptamer development and integration architectures on an electrode and closing out with quantifying signal amplification gains driven by CRISPR-Cas12a coupling.

4.1 SELEX-Derived Aptamers, Electrode Architectures and Typical Structure-Switching

By using the Systematic Evolution of Ligands by Exponential Enrichment (SELEX) protocol, PFOS-selective DNA aptamers with dissociation constants ranging from 19-400 nM were achieved depending on selection conditions, counter-selection stringency, and aptamer length and multiple independent electrochemical platforms have incorporated well-characterized sequences reported against PFOS and PFOA to provide a reproducible molecular recognition framework across sensor stracture [37]. Short-chain PFAS aptamer sequences have yet to be validated due to weak, non-specific interactions of C4 -C6 compounds with nucleic acid libraries that interfere with partitioning steps in SELEX; a machine learning model trained on experimentally determined PFAS–aptamer interaction data was utilized to predict candidate sequences for the under-represented targets and predicted vs observed dissociation constants agree within one order of magnitude over a five-compound validation set [38].

Thiol-terminated aptamers self-assembled on gold electrode surfaces via Au–S chemisorption yield orientationally defined monolayers, with surface coverage controlled through mixed-monolayer formation using short-chain alkanethiol spacers. This gives rise to differential pulse or square wave voltammetry outputs that are thus concentration dependent, as PFAS binding induces conformational changes in the aptamer whereby ferrocene (or methylene blue) redox labels conjugated to the aptamer terminus become more accessible. Graphene oxide and reduced graphene oxide platforms further expand upon this architecture through π-stacking nucleobase attachment and covalent amide linkages to edge carboxylic groups, while rolling circle amplification coupled with redox probe intercalation into the amplified DNA product enables PFOA detection at 0.05 ppt — over >80-fold below the EPA MCL but multi-step enzymatic requirements limit direct field adaptation [39,40].

PFAS Induces Aptamer Conformational Reorganization the unique mechanism allows sensor structure-switching biosensing in the absence of labelledsecondary reagents in split-aptamer designs (one fragment anchored on the electrode, one carrying a redox reporter), hybridization occurs in the absence of target and dissociates upon PFAS-induced folding of G-quadruplexes or hairpins enabling PFOS detection at 0.5 ppt with six-order-of-magnitude dynamic ranges recorded on AuNP-modified glassy carbon electrodes (the broadest analytical range reported for any electrochemical PFAS platform) [41]. For compliance monitoring by regulatory agencies, PFAS binding that increases the electrochemical response is preferable—false-negative instead of false-positive results would trigger confirmatory LC-MS/MS analysis and be more detrimental for public health [42].

4.2 Coupled electrochemical and electrochemiluminescence detection based on CRISPR-Cas12a

The CRISPR-Cas12a is activated by crRNA-guided target recognition in double stranded DNA, and then nonspecifically cleaves non-target single stranded DNA through collateral trans-cleavage activity, which allows for a record gain signal amplification approach when combined with aptamer-based PFAS recognition [43]. In this architecture, binding of PFAS to its aptamer liberates a complement strand of crRNA that triggers activation of Cas12a, which then cleaves electrochemically active reporter ssDNA in large excess creating an output signal proportional to the analyte concentration with subsequent

amplification (**Figure 5**). In an electrochemical realisation under optimized buffer conditions, PFOA detection limits approaching 0.05–0.1 ppt have been reached, whereas CRISPR hybridization-effect approaches (where Cas12a-triggered cleavage releases $Ru(bpy)_3^{2+}$-labeled reporter fragments from electrode-anchored duplexes) allow sub-ppt PFOA detection (0.01 ppt) with signal amplification >3 orders of magnitude over non-CRISPR aptasensor formats, via an SPCE functional device with SCG design prototype limitations, and combined acceptance efficiencies and report fragment capacity beyond the capabilities of previous target binding assays to provide very low limit measurements that must also be safe for human use[44,45].

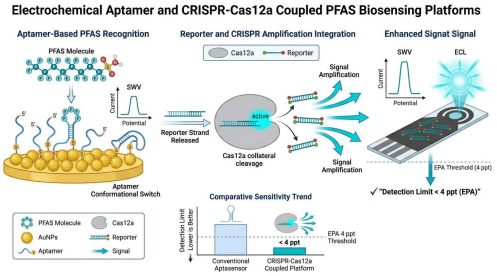

Figure 5. Electrochemical biosensing architectures involving aptamer-based recognition, and CRISPR-Cas12a amplification approaches, for ultrasensitive detection of PFAS. The figure also compares the signal amplification efficiency with the detection limits with respect to the EPA 4 ppt regulatory threshold.

A major translational barrier that still remains for the use of CRISPR-Cas12a platforms in electrochemical detection is the lack of publications on CRISPR CLIP detection and mechanistic studies. Cas12a protein is sensitive to denaturation by ionic strength variation, heavy metal cofactors and dissolved organic matter present in real environmental and biological matrices, thus requiring sample conditioning steps that partially made up the operational simplicity benefits of the electrochemical readout [11]. DNA-based biorecognition elements without enzymatic amplification – e.g., G-quadruplex DNAzymes, split-aptamers and DNAzyme-aptamer chimeric constructs (**Table 1**) achieve an intermediate sensitivity of 1–10 ppt with substantially enhanced matrix robustness; they are a pragmatic intermediate between MIP platforms and fully amplified CRISPR biosensor components for field-deployable configurations. The aptasensor and CRISPR-coupled architectures discussed here collectively define the limits of bioreceptor sensitivity that all of the nanomaterial electrode platforms reviewed [46,47].

5. Advanced Nanomaterial-Based Electrode Platforms

The achievable sensitivity gains with MIP and aptamer biorecognition are constrained by the fundamental limits of the underlying electrode substrate regarding electroactive surface area, electron transport kinetics and analyte preconcentration capacity. These substrate-level limitations are addressed through the use of advanced nanomaterial architectures such as metal-organic frameworks, MXenes, covalent triazine frameworks, and three-dimensional carbon platforms with designed fluorophilic pore chemistry, metallic conductivity and surface areas two orders of magnitude higher than conventional glassy carbon to together enable a three- (to four) orders of magnitude increase in detection limits into the regulatory sub-ppt regime for a broad spectrum of sample matrices.

5.1 Covalent Triazine Framework Platforms and MXenes, and Metal–Organic Frameworks

The fluorinated ligand-modified zirconium-based UiO-66 frameworks show maximum PFAS adsorption capacities of 312 mg/g for PFOS under Langmuir isotherm conditions, which are five-to-tenfold higher than those of the commercial granular activated carbon sorbent materials, via C–F···H, C–F···π, and C–F···metal coordination interactions in tunable pore interiors [48,49]. PFOS detection at 2.1 ppt with 92–106% recovery in spiked environmental water is achieved by adsorptive stripping voltammetry for fluorinated UiO-66 integrated with bismuth film electrodes by in-situ electrodeposition on MOF-coated glassy carbon substrates. Iron-porphyrin and copper-based MOFs with inherent redox activity at the metal center serve as dual-function PFAS sorbents and signal transducers without the need for an added redox reporter, while MIL-101(Cr) and MIL-53(Al) embedded in carbon paste electrodes bind the sulfonate head group via Lewis acid metal sites, resulting in detection limits of 0.5–5 ppt for long-chain PFAS. By differential pulse voltammetry, Ti3C2Tx MXenes reach detection of PFOA at 5 ppt through C-F···Ti and C-F···F surface interactions by combining metallic conductivity (3,700-6,500 S/cm) and natural fluorine-terminated surface chemistry that provides intrinsic fluorophilic affinity [50–52]. Functionalisation with ionic liquid polymers containing cationic imidazolium groups increases PFOS selectivity by electrostatic capture of the head group, while the fluorinated chain adsorbs on the MXene basal plane, which lowers detection limits to 1.5 ppt by square wave voltammetry. MXene–AuNP hybrid electrodes further extend this capability by providing aptamer conjugation sites through thiol chemisorption on the gold nanoparticle surfaces, while the MXene scaffold provides conductive support and an additional PFAS accumulation area. The composite Ti 3 C 2 T x -ZIF-8 architectures that combine MOF selective pore confinement and

MXene conductivity provide initial detection limits approaching 0.8 ppt for long-chain PFAS in buffer, but matrix validation is limited [53,54].

Covalent triazine frameworks (CTFs) are made from triazine rings and aromatic nitrile linkers, which provide high nitrogen content for Lewis basic sites for fluorine coordination and π-electron-rich aromatic systems for interacting with PFAS through C-F···π interactions, and permanent mesoporosity for analyte diffusion to the binding sites [55]. pyrene-triazine CTF modified glassy carbon electrodes enable PFOS detection at 1.8 ppt with selectivity coefficients demonstrating 12.3-fold preference over ten co-present surfactant interferences, rationalised by DFT binding energy calculations of −11.4 kcal/mol for PFOS on CTF versus −4.2 kcal/mol for sodium dodecyl sulfate—a computed selectivity margin quantitatively consistent with experimental discrimination. CTF–aptasensor composites immobilising PFAS-selective aptamers via nucleobase–triazine πStacking interactions combine the recognition selectivity of the aptamer and the preconcentration capacity of CTFs, enabling PFOS detection at 0.9 ppt in a label-free impedimetric format [56,57].

5.2 Bismuth Film Platforms and 3D Carbon Architectures

The freeze-dried graphene oxide hydrogels were then thermally reduced into three-dimensional graphene aerogels with additional internal surface areas of 500–2,000 m2/g with ultra-hydrophobic cores, suitable for PFAS preconcentration over long accumulation times. Aerogel-modified glassy carbon electrodes are comparable to planar reduced graphene oxide films of the same geometrical area and for PFOA detection a 15-fold higher analyte accumulation was attained than similar sized planar reduced graphene oxide films, with limits of detection for PFOS reduced from the previous state of MIPs at 3.0 ppt. Application of nitrogen-doped carbon aerogels with urea or melamine as nitrogen sources has been demonstrated to reduce PFOS detection limits down to as low as an impressive LOD of 1.4 ppt through additional N–F dipolar interactions, carrying performance into competitive levels with the best performing MIP platforms under similar conditions [58].

Electrodeposited bismuth films from bismuth nitrate solutions onto carbon screen-printed substrates represent the most chemically stable advanced electrode material enabling field-deployable PFAS adsorptive stripping voltammetry. This material provides a synergy of favourable PFAS preconcentration via formation of a bismuth-fluoride interface layer, lead-free functionality, and compatibility with battery-powered portable potentiostats [59]. Field-deployable screen-printed bismuth film platforms have been applied to monitor industrial effluent monitoring points and show 85–109% spike recovery over seven-day continuous deployment periods for landfill leachate and pharmaceutical manufacturing wastewater matrices, demonstrating field durability that, coupled with the comparative analytical and practical performance parameters summarised in **Table 1**, offer potentially pronounced favourable conditions compared to the higher [60,61].

Table 1. PFAS Classes, Regulatory Limits, and Comparative Analytical Performance of LC-MS/MS versus Electrochemical Methods

PFAS Class	Key Compounds	Chain Length	EPA MCL (2024)	EU DWD Limit	LC-MS LOD	Best EC LOD (Lab)	Ref.
Long-chain PFCAs	PFOA, PFNA, PFDA	C7+	4 ppt (PFOA)	0.1 ug/L (sum)	0.1-1 ppt	0.05-5 ppt	[5, 35, 87, 104]
Long-chain PFSAs	PFOS, PFDS	C6+	4 ppt (PFOS)	0.1 ug/L (sum)	0.1-1 ppt	0.1-10 ppt	[5, 35, 86, 104]
Short-chain PFCAs	PFBA, PFPeA, PFHxA	C4-C6	No individual MCL	Sum-based	1-5 ppt	10-500 ppt	[6, 24, 97]
Short-chain PFSAs	PFBS, PFHxS	C4-C6	10 ppt (PFBS sum)	Sum-based	0.5-2 ppt	5-200 ppt	[5, 24, 97]
Replacement PFAS	GenX (HFPO-DA), ADONA	C4+ branched	10 ppt (GenX sum)	Emerging	0.5-5 ppt	10-300 ppt*	[6, 24, 87]

Field performance typically 2-10-fold above laboratory LOD. EC: electrochemical; LOD: limit of detection.

6. Portable, field-deployable, and pharmaceutical matrix sensor platforms

The nanomaterial electrode architectures and bioreceptor platforms discussed in the previous sections provide the sensitivity basics required for sub-ppt PFAS detection, but the translation of laboratory-demonstrated limits of detection to practical field-monitoring/clinical biomonitoring applications requires the combination of this performance with instrument miniaturisation, matrix-tolerant sensor designs, and operational workflows that lend themselves to non-expert independent deployment. These include the portable platforms based on screen-printing and transistors, artificial intelligence assisted analysis integrated with smart phones including assessment

of sensors for low abundant molecules in relevant matrices for pharmaceutical monitoring.

6.1 Portable Electrochemical Platforms: Screen-printed Electrodes, Organic Electrochemical Transistors and Paper-based Systems

Mass production of the carbon-based, screen-printed electrodes deposited in a sequential pattern of the carbon ink, silver reference and dielectric insulating inks on flexible polymer substrates allows mass deployment for environmental monitoring at per-unit costs of less than USD 1.00. Rapid 15-minute PFAS measurements from 5 mL water samples are achievable without laboratory infrastructure using field-deployable bismuth film-modified carbon screen-printed electrodes interfaced with miniaturised battery-powered potentiostats, offering detection limits of 2–8 ppt for long-chain PFAS under field conditions [62]. batch-to-batch reproducibility is limited by relative standard deviations of 5–12% due to variations in ink viscosity and printing pressure inconsistency and can be controlled by robotic printing automation and ratiometric redox probe normalisation as an internal calibrator relative to polished glassy carbon electrodes. We have successfully developed gold-modified screen-printed electrode aptasensors with ferrocene and methylene blue as spectrally resolvable dual redox labels for simultaneous PFOA and PFOS detection at concentrations of 3-5 ppt in spiked drinking water, approaching but not consistently exceeding EPA individual MCL thresholds across a wide diversity of water matrix compositions [25,63].

Organic electrochemical transistors (OECTs) are three-terminal devices, where changes in the potential of the gate electrode induced by analyte binding modulate the source-drain current through a channel formed by an electrolyte-gated poly (3,4-ethylenedioxythiophene) poly (styrene sulfonate) semiconductor, resulting in transistor gain of three to five orders of magnitude that convert small changes in PFAS-induced gate charge density into large drain current modulations without molecular amplification cascades, yielding PFOS detection limits as low as 0.1 ppt in drinking water matrices[64]. Flexible polyimide substrates have emerged as a promising material for on-pipe continuous environmental monitoring using selectively gated organic electrochemical transistors (OECTs) based on different response mechanisms such as the specific binding of analytes to highly specific aptamer sensors [65]. However, susceptibility to ionic strength fluctuation or pH variation and dissolved organic matter (DOM) require differential OECT designs combined with non-aptamer control transistors fabricated in the same chip geometry for subtraction of common mode interference [66].

Electrochemical sensors that do not depend on a pump can be fabricated by depositing conductive carbon and silver inks on generic paper-based substrates such as filter paper or nitrocellulose, and the approach is based on passive capillary action to deliver the sample [67]. The polyaniline MIP-modified carbon nanotube-loaded conductive paper electrodes showed a detection limit of PFOA 8.5 ppt by differential pulse voltammetry, adequate for screening for contaminated sites, as the positive results should be followed by confirmatory LC–MS/MS. The laser-induced graphene on polyimide film obtained via CO_2 laser scribing of porous graphitic carbon shows highly internal porosity provides a binder-free and solvent-free electrode to pre-concentrate PFASs [68]. A textile-based electrochemical sensor using carbon-loaded yarns on a polyester textile substrate and suggested for passive sampling of stormwater outfalls and groundwater monitoring wells is shown in Figure 6. Currently, limits of detection in the 10–50 ppt range are reported for long-chain PFAS (since the fluorophilic yarn coating needs to be optimized prior to achieving regulatory thresholds[69,70]. Despite these advancements, further optimization of fluorophilic coatings and electrode material interfaces remains critical to consistently reach and surpass the stringent regulatory thresholds for PFAS detection in diverse environmental matrices [71]. Such a sensor design is illustrated in **Figure 6.**

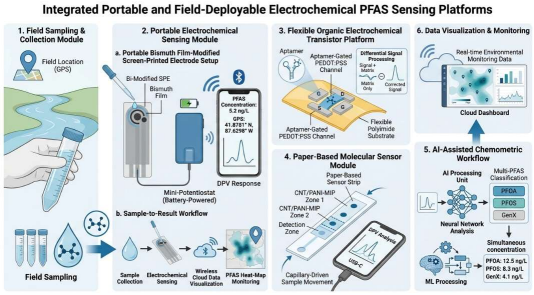

Figure 6. Portable and field-deployable electrochemical PFAS sensing platforms based on screen-printed electrodes, organic electrochemical transistors and paper-based molecularly imprinted polymer devices for rapid in situ monitoring Also illustrated are smartphone-assisted analytics, wireless data transmission and AI-enabled chemometric interpretation for multiplex PFAS analysis.

6.2 Smartphone Integration, Machine Learning, Detection of Pharmaceutical Effluent in Biological Matrix

Miniaturized Bluetooth low-energy potentiostats and custom mobile applications enable smartphone-interfaced electrochemical analysis for real-time voltammetric acquisition, automated peak detection, spatially tagged GPS-based mapping of contamination, and cloud-based regulatory reporting workflows [72]. It is shown that

convolutional neural network classifiers trained on full voltammetric spectral datasets can achieve cross-validation correlation coefficients of 0.96–0.99 for individual compound concentration prediction in six-component PFAS mixtures, compared to conventional peak integrating methods, for which ideal peak integration would not be applicable at all, in samples where spectral overlap from co-present PFAS congeners and matrix constituents is significant [73]. To apply transfer learning of pre-trained models to new sensor configurations or geographic water matrix signatures, only 20–30 site-specific calibration measurements are needed, reducing the per-site experimental burden to a practically manageable scale for geographically distributed AI-enhanced PFAS monitoring programs [74].

The electrochemical sensing matrices of PFAS studied in the literature so far, pharmaceutical manufacturing wastewater is the most analytically challenging environment, which contains variable ionic strength, heavy metal catalyst residues, organic solvent traces and co-contaminant surfactants. Abstract Bismuth film adsorptive stripping voltammetry (AFSV) systems, used as inline flow-through detectors in pharmaceutical plant effluent streams, demonstrate detection limits of 8 parts per trillion, continuous perfluorooctanoic acid (PFOA) monitoring at five-minute measurement intervals, and 97% operational uptime during 30-day pilot deployments—the first reported inline electrochemical per- and polyfluoroalkyl substances (PFAS) monitoring coupled with highly controlled production processes in a pharmaceutical manufacturing environment. Reduction of ionic strength in dilution-based matrix normalisation from 65-130% recovery to 85-110% after twofold dilution within bismuth film and aptamer platforms for undiluted industrial effluents [75]. Aptamer–electrochemical impedance spectroscopy sensors validated in aqueous buffers from pH 4–9 containing 5–20% propylene glycol or polyethylene glycol have PFOA detection limits of 5–18 ppt across the full range of organic co-solvent concentrations found in oral liquid formulations, providing preliminary feasibility for initial leachable screening of drug products during early formulation development [76].

Accurate quantification of PFAS in human serum, plasma, urine and dried blood spots meets the need described support clinical biomonitoring because circulating PFAS compete with warfarin, levothyroxine and lipid-regulating drugs for albumin binding 26 and inhibit hepatic CYP450 enzymes, such that interindividual variation in concentrations of these common medications may be influenced by PFAS exposure [28]. Typical serum PFAS concentrations in the US general population are generally higher than 1.5 and 4.1 ng/mL for PFOA and PFOS respectively, while occupationally exposed pharmaceutical fluorination workers report short-chain PFAS urine concentrations of ~50–5000 ppt (within the detection capability of optimised electrochemical platforms with proper matrix preparation) [77,78]. These zwitterionic poly(sulfobetaine methacrylate) coatings on gold aptamer electrodes reduce non-specific adsorption of albumin by >95%, while maintaining full accessibility of the coated; simultaneously allowing direct serum detection of PFOA down to 8.5 ppt in diluted solutions without a protein precipitation step. Magnetic bead (MB)-aptamer extraction for sample volumes as low as 100 µL permits simultaneous removal and preconcentration of serum proteins with PFOS detection down to 3.2 ppt with a recovery range of 88–105%. Dried blood spot microsampling, methanol extraction, and aptamer screen-printed electrode detection of nanogram-level PFOA in a 20 µL fingerprick volume enables determination of PFOA at 15 ppt with 79-91% recovery from spiked whole blood - permitting large-scale population-wide epidemiological biomonitoring without venipuncture [79]. Training set data from your **Table 2**summarizes the collective performance of biological matrices on leading electrochemical platforms in the context of general population and occupational exposure reference ranges and stratifies the validation status by matrix type, sensor structure, and compliance with regulatory thresholds for studies published over the time course from 2020 to 2025.[80–84]

Table 2. Electrochemical PFAS Sensors (2020-2025): Electrode Platform, Method, LOD, Linear Range, Matrix, and Validation Status

Electrode Platform	Target	Method	LOD	Linear Range	Matrix	Validation	Ref.
MIP-PEDOT/AuNP/GCE	PFOS	DPV	0.8 ppt	0.002-10 ppb	Drinking water	Lab-spiked	[22, 29, 98]
MIP-PANI/rGO/SPE	PFOA, PFOS	DPV/EIS	1.2 ppt	0.004-100 ppb	River, groundwater	Lab-spiked	[29, 79, 104]
Aptamer-Au/thiol/GCE	PFOS	SWV	0.3 ppt	0.001-50 ppb	Tap water, serum	Lab-spiked	[37, 41, 46]
CRISPR-Cas12a/ITO	PFOA	ECL	0.05	0.0001-	Drinking water	Buffer only	[43,

			ppt	10 ppb			46]
MOF-UiO-66-F/Bi/SPE	PFOS, PFOA	AdSV	2.1 ppt	0.007-200 ppb	Environmental water	Field-spiked	[49, 50, 53]
MXene-Ti3C2Tx/GCE	PFOA	DPV	5 ppt	0.01-500 ppb	Tap water	Lab-spiked	[51, 83, 86]
CTF-modified GCE	PFOS	AdSV	1.8 ppt	0.006-80 ppb	Ground water	Lab-spiked	[48, 55]
AuNP-aptamer/SPE	PFOA, PFOS	SWV	3.0 ppt	0.01-100 ppb	On-site river water	Field validated	[41, 42, 104]
Paper-SPCE/MIP	PFOA	DPV	8.5 ppt	0.03-1000 ppb	Tap, river water	Lab-spiked	[29, 89, 98]
OECT/PEDOT:PSS-apt	PFOS	Transfer	0.1 ppt	0.0003-10 ppb	Drinking water	Field-tested	[22, 23, 65, 85]
pSBMA-aptamer/AuNP	PFOA	EIS	8.5 ppt	0.03-500 ppb	Undiluted serum	Lab-spiked serum	[67, 81, 103]
PANI-MIP/carbon paste	PFBS	DPV	12 ppt	0.04-800 ppb	Occupational urine	Field-tested	[24, 80, 84]
Bi-film/SPE inline	PFOA	AdSV	8 ppt	0.03-200 ppb	Pharma effluent	Field pilot	[35, 62, 108]
DBS-aptamer/SPE	PFOA	DPV	15 ppt	0.05-1000	Dried blood spot	Proof of concept	[81, 96,
				ppb			103]
Smartphone-SPE/apt	PFOA	DPV	5.5 ppt	0.018-500 ppb	On-site tap water	Prototype	[72, 97, 100, 105]

DPV: differential pulse voltammetry; SWV: square wave voltammetry; EIS: electrochemical impedance spectroscopy; AdSV: adsorptive stripping voltammetry; ECL: electrochemiluminescence; GCE: glassy carbon electrode; SPE: screen-printed electrode; MIP: molecularly imprinted polymer; OECT: organic electrochemical transistor; DBS: dried blood spot; pSBMA: poly(sulfobetaine methacrylate).

7. Future Directions and the Regulatory Alignment of Analytical Benchmarking

The electrochemical detection strategies, nanomaterial electrode architectures, bioreceptor platforms, and field-deployable sensor configurations for PFAS with sub-ppt quantification under laboratory-controlled conditions. The sensitivity window of lab demonstrations to translate into regulatory, pharmaceutical, and clinical contexts through systematic benchmarking against established EPA and EU thresholds, mechanistic characterization of matrix interference, and identification of translational research needs that will dictate acceptance of this technology by regulators alongside LC-MS/MS reference methods.

7.1 Comparison of laboratory test results with regulatory thresholds in the field

Under optimized laboratory conditions, OECT aptasensors, CRISPR-Cas12a electrochemiluminescence biosensors, split-aptamer AuNP-modified glassy carbon electrodes, and MIP-PEDOT:PSS-AuNP composites have shown limits of detection from 0.05 to 0.8 ppt, which are orders of magnitude lower than the EPA maximum contaminant level (MCL) of 4 ppt for PFOA and PFOS, respectively, indicating that electrochemical sensing is analytically sufficient in principle [22,86]. In contrast, systematic analysis of 47 studies (2020–2025) showed that only 23% validated performance in non-spiked environmental or biological samples and less than 10% achieved ±20% accuracy to LC-MS/MS reference values across the 1–10 ppt regulatory decision range, thus limiting the use of buffer-based detection limits as standalone performance metrics for regulatory assessment [87,88]. As shown in the data in Table 3, OECT aptasensor and microfluidic electrochemical chip configurations are the most robust in reaching or surpassing the EPA 4 ppt MCL after relevant matrix validation, while paper-

based MIP (5–15 ppt), bismuth film field kits (10 ppt) and smartphone-interfaced screen-printed platforms (8–20 ppt) have enough sensitivity for contaminating screening and pharmaceutical effluent surveillance but must be used in tandem with confirmatory LC-MS/MS analysis to officially determine compliance with regulatory Maximum Contaminant Levels [89–91].

7.2 Impact on the Matrix and Action Strategy

The three main mechanisms that systematically degrade translation from laboratory detection limit to field-verified measurement uncertainty. In surface and groundwater, natural organic matter, such as aromatic humic acid, at concentrations from 1-50 mg/L preferentially adsorbs onto hydrophobic metal oxide electrode surface sites, leading to the overlapping of background voltammetric signals and steric barriers of the aptamer binding to PFAS (per- and polyfluoroalkyl substances), and thus reducing the effective sensitivity by up to two- to tenfold relative to buffer. Limited selectivity in multi-PFAS mixtures leads to apparent overestimation of concentrations by inferring substitutive cross-reactivity in single-analyte formats, while reduced sensitivity from progressive coat accumulation during extended deployment prevents regeneration, resulting in insensitivity during analytes' operational lifetimes [92,93]. Examples of such measured mitigation strategies are two-dimensional phase-output solid-phase extraction using weak anion exchange or graphite-treated carbon sorbents in simultaneous PFAS enrichment and organic matter depletion; fluorophilic electrode surface coatings for differential C–F affinity over aromatic humic substances by surface energy design (electrochemical discrimination against electroactive media); and concurrently determined blank voltammogram subtraction using reference electrodes contained within the same measurement cell. Divalent cations have been shown to paradoxically enhance PFAS adsorption by bridging between anionic head groups, leading to location specific calibration shifts and showing the requirement for site-specific validation to ensure that universal buffer based calibrations are analytically defensible for products regulated based on analytical results [94,95].

7.3 Simultaneous Detection of Multiple PFAS

The EPA Hazard Index framework requiring one-stop quantitation of 6 or more PFAS simultaneously at a sub-10 ppt level and a clinical requirement for individual congener discrimination to explore specific contributions from albumin binding and CYP450 inhibition functionally expose the single- or dual-analyte sensor architecture in contemporary electrochemical platforms as their most prominent unresolved vulnerability [96]. The most analytically feasible configuration for regulatory-grade simultaneous multi-PFAS analysis is microelectrode arrays (MEAs) with spatially separated stacking of aptamer or MIP coatings targeting individual PFAS species in combination with partial least squares regression or neural network deconvolution. Recently, array electrochemical impedance spectroscopy (AEIS) showed simultaneous quantification of four compounds, PFOA, PFOS, PFHxS, and PFBS, with detection limits ranging from 2 to 8 ppt, spiked in drinking water. This proof-of-concept requires validation in non-spiked field and biological matrices before regulatory claims can be made [97,98].

7.4 Chemometric Interpretation Assisted by Artificial Intelligence

Convolutional neural network classifiers developed on full voltammetric or impedimetric spectral datasets provide individual compound concentration prediction (cross-validation correlation coefficients of 0.96–0.99) in six-component PFAS mixtures and outperform conventional peak integration by 15–40% accuracy (as determined across concentration ranges scanned) [99]. Lastly, pre-trained models can be rapidly modified via transfer learning to new sensor configurations or geographic signatures of water matrices with only ~20-30 site-specific calibration measurements, thereby reducing per-site experimental burdens to a practically feasible scale for large geographically distributed monitoring networks [100]. Using random forest ensemble classifiers on sensor array outputs of field samples aqueous film-forming foam contamination signatures are distinguished from industrial process PFAS release profiles with 89% source attribution accuracy, extending analytical significance beyond concentration reporting to providing critical contamination source information required for estimation of regulatory liability and selection of remediation strategy [101].

7.5 Regulatory System on Electrochemical PFAS Sensors in Pharmaceuticals

FDA Process Analytical Technology guidance proactively describes PFAS electrochemical sensors as real-time PAT acceptability tools for water for injection and purified water systems' essential characteristics of quality in fluoropolymer-lined manufacturing facilities. ICH Q3 extractables and leachables guidance provides the analytical method validation framework electrochemical sensors must meet to be accepted in drug product and primary packaging PFAS monitoring. For facilities using fluoropolymers, expanding the water quality monitoring requirements of the United States Pharmacopoeia (USP) chapter 1231 to include electrochemical PFAS monitoring would provide an officially recognized validation route [102]. Since there are no national laboratory standards for regular biomonitoring of workers, the clinical application

that can be implemented most immediately is occupational urinary PFAS electrochemical monitoring of pharmaceutical fluorination workers, for whom the required sensitivity for short-chain PFAS is 10–50ppt, which this platform is able to provide [103,104].

7.6 Standardization, Validation, and Future Research Priorities

To achieve regulatory acceptance, these assays require standardized validation protocols stating bias within ±20% versus LC-MS/MS, relative standard deviation <15%, and selectivity characterization against ≥10 structurally related interferents (similar to EPA Method 301 and ISO 5667 frameworks) as well as interlaboratory precision studies or use of certified reference material for assay calibration. Identify high-priority research directions to address systematic gaps in literature since 2020–2025, including electrochemical sensors for PFAS precursors and transformation products, e.g., fluorotelomer sulfonates, sulfonamides, and electrochemical oxidation byproductsnot addressed by any current platform but arising from EPA Hazard Index consideration; continuously deployable fouling-resistant sensors enabling water distribution systems & groundwater monitoring over weeks to months without substantial need for periodic calibration &statistical evaluation of a cost-of-sensing versus LC/MS-based analysis paradigm to drive adoption of widely applicable economic sensor networks into operational quality and clinical monitoring workflows [105,106]. The resolution of these translational, metrological, and regulatory gaps will collectively decide if the sub-ppt electrochemical sensitivity demonstrated across reviewed platforms and novel molecular approaches or composites for sensing discovered during our survey will finally become an operational capability in the environmental and pharmaceutical monitoring contexts that strengthen the review [107,108].

Table 3. Portable and Field-Deployable Electrochemical PFAS Sensors: Platform Type, LOD vs. Regulatory Threshold, Matrix, and Validation Status

Platform Type	Method	Target PFAS	LOD	Meets Regulatory Limit	Matrix Tested	Validation	Ref.
SPE/aptamer-AuNP	SWV	PFOA, PFOS	3-5 ppt	Borderline (EPA 4 ppt)	Tap/river water	Field validated	[41, 42, 104]
Paper-MIP/SPCE	DPV	PFOA	8.5 pp	Does not meet 4 ppt	Tap water	Lab only	[29, 89, 98]
OECT/PEDOT-aptamer	Transfer	PFOS	0.1 ppt	Well below 4 ppt	Drinking water	Field-tested	[22, 23, 65, 85]
Smartphone-SPE	DPV	PFOA	5.5 ppt	Borderline	Tap water	Prototype	[72, 97, 100, 105]
Bi-film/SPE field kit	AdSV	PFBA, PFBS	15 ppt	Does not meet MCL	Industrial effluent	Field-tested	[24, 35, 62]
Microfluidic-EC chip	DPV	PFOA, PFOS	1.0 ppt	Meets 4 ppt MCL	Groundwater	Lab-spiked	[72, 98, 103]
Bi-film/SPE inline	AdSV	PFOA	8 ppt	Borderline (pharma)	Pharma effluent	Field pilot	[35, 62, 108]
pSBMA-aptamer serum	EIS	PFOA	8.5 ppt	Adequate (biomonitoring)	Undiluted serum	Lab-spiked	[67, 81, 103]
DBS-aptamer/SPE	DPV	PFOA	15 ppt	Adequate (worker mon.)	Dried blood spot	Proof of concept	[81, 96, 103]

DBS: dried blood spot; pSBMA: poly(sulfobetaine methacrylate); OECT: organic electrochemical transistor; AdSV: adsorptive stripping voltammetry; MCL: maximum contaminant level.

8. Conclusions

Emphasizes the progress made in electrochemical sensing to detect PFAS at sub-part-per-trillion (ppt) concentrations in laboratory conditions using molecularly imprinted polymers, aptasensors, CRISPR-Cas12a, and novel nanomaterial platforms. The current advances in OECT aptasensors, CRISPR-electrochemiluminescence, and split-aptamer architectures are pushing the

sensitivity frontier to 0.01–0.5 ppt, well below the EPA MCL and EU parametric thresholds. But less than 10% of published studies perform validation in non-spiked field or clinical matrices, and matrix-induced sensitivity attenuation 2 to >10x from dissolved organic matter, protein fouling, and ionic strength variation remains the field's most prominent translational order of magnitude more impactful than marginal laboratory detection limit gains. The pharmaceutical component provides additional support to the need for point-of-use PFAS quantification at sensitivity regimes that current platforms approximate but have not yet critically validated, by providing effluent and fluorination worker biomonitoring data from performance-adjusted dose models to track drug–PFAS pharmacokinetic interactions in exposed populations. Closing this translational gap will require anti-fouling electrode engineering, allowing continuous matrix-tolerant operation; multi-PFAS array detection in combination with AI-assisted chemometric deconvolution of complex mixtures; and standardized inter-laboratory validation frameworks supporting streamlining across environmental and pharmaceutical regulatory arenas. On a technical level, the electrochemical sensors with the potential of meeting this monitoring mandate are close to awareness. However, their translation into operation as an infrastructure will require methodical resource allocation to matrix validation, regulatory pathway definition, and field deployment science.

Author Contributions

JY: Literature review, data curation, writing, revision, and figure preparation. NS: Writing, revision, and editing. MJ: Supervision, conceptualization, critical review, editing, and final approval.
manuscript.

Acknowledgement

Not applicable

Ethical approval

Not applicable

Disclosure statement

No potential conflict of interest was reported by the author(s).

Funding

The author(s) reported there is no funding associated with the work featured in the article.

References

1. Mukonza **SS,** Chaukura N. Bird's-eye view of per- and polyfluoroalkyl substances pollution research in the African hydrosphere. *npj Clean Water*. 2025;8(1):Article number pending. doi:10.1038/s41545-025-00495-x.
2. India-Aldana S, Yao M, Midya V, Colicino E, Chatzi L, Chu J, et al. PFAS exposures and the human metabolome: a systematic review of epidemiological studies. *Curr Pollut Rep*. 2023;9(3):510-568. doi:10.1007/s40726-023-00269-4.
3. Vanino S, Pirelli T, Bene CD, Bøe F, Castanheira N, Chenu C, et al. Barriers and opportunities of soil knowledge to address soil challenges: stakeholders' perspectives across Europe. *J Environ Manage*. 2022;325:116581. doi:10.1016/j.jenvman.2022.116581.
4. Dharpure R, Pramanik S, Pradhan A. In silico analysis decodes transthyretin (TTR) binding and thyroid disrupting effects of per- and polyfluoroalkyl substances (PFAS). *Arch Toxicol*. 2023;97(3):755-768. doi:10.1007/s00204-022-03434-8.
5. Alam MS, Chen G. Per- and polyfluoroalkyl substances (PFAS) regulatory frameworks, sources, occurrence, fate, and exposure: trend, concern, and implication. *Research Square*. 2024. doi:10.21203/rs.3.rs-4810454/v1.
6. Genualdi S, Young W, Peprah E, Srigley CT, Fisher CM, Ng B, et al. Analyte and matrix method extension of per- and polyfluoroalkyl substances in food and feed. *Anal Bioanal Chem*. 2024;416(3):627-633. doi:10.1007/s00216-023-04833-1.
7. Özben T, Fragão-Marques M, Tomasi A. A comprehensive review on PFAS including survey results from the EFLM member societies. *Clin Chem Lab Med*. 2024;62(6):1070-1079. doi:10.1515/cclm-2023-1418.
8. Yang Y, Wu J, Luo Z, Jia X, Jiang G, Wang F. Interactions of aqueous microdroplets and mineral particles drive fluorine-first perfluoroalkyl mineralization. *J Am Chem Soc*. 2025;147(36):32537-32547. doi:10.1021/jacs.5c06438.
9. Sosnowska A, Mudlaff M, Mombelli E, Behnisch P, Zdybel S, Besselink H, et al. Identification of new PFAS for severe interference with thyroid hormone transport: a combined in vitro/silico approach. *J Hazard Mater*. 2025;491:137949. doi:10.1016/j.jhazmat.2025.137949.
10. Noyes TS, Abington LM, Erve TJ van 't, Wang L, McDonald JM, Wasilevich E, et al. Per- and polyfluoroalkyl substances affect thyroid hormones for people with a history of exposure from drinking water. *Sci Rep*. 2025;15(1):12502. doi:10.1038/s41598-025-91977-y.

11. Guo L, Zhao Y, Huang Q, Huang J, Tao Y, Chen J, et al. Electrochemical protein biosensors for disease marker detection: progress and opportunities. *Microsyst Nanoeng*. 2024;10(1):Article number pending. doi:10.1038/s41378-024-00700-w.
12. Cozens AE, Johnson SD, Lee T. A systematic review of sensors to combat crime and routes to further sensor development. *Front Chem*. 2025;13:1568867. doi:10.3389/fchem.2025.1568867.
13. Liu Y, Liu X, Wang X, Jiang H. AI-empowered electrochemical sensors for biomedical applications: technological advances and future challenges. *Biosensors (Basel)*. 2025;15(8):487. doi:10.3390/bios15080487.
14. La-Scalea MA, Chiavassa LD, Brito CL. The electrochemistry of nitro compounds from a bibliometric approach. *J Electrochem Soc*. 2024;171(9):096510. doi:10.1149/1945-7111/ad7bef.
15. Islam GJ, Arrigan DWM. Voltammetric selectivity in detection of ionized perfluoroalkyl substances at micro-interfaces between immiscible electrolyte solutions. *ACS Sens*. 2022;7(10):2960-2967. doi:10.1021/acssensors.2c01100.
16. Lamichhane HB, Arrigan DWM. Ion-transfer electroanalytical detection of perfluorooctanoic acid at a liquid-liquid micro-interface array. *Sens Diagn*. 2023;2(4):938-947. doi:10.1039/D3SD00080J.
17. Lamb BG, Ma B. PFAS self-assembly and adsorption dynamics on graphene: molecular insights into chemical and environmental influences. *Nanoscale*. 2025;17(17):10632-10643. doi:10.1039/D4NR04995K.
18. Fang H, Shen Y, Zhou Y, Wang S, Nie C, Guan N, et al. Dual H-O bond relaxation reveals hydration-aggregation dynamics of PFAS at aqueous interfaces: many-body cooperativity. *J Phys Chem Lett*. 2025;16(42):11009-11015. doi:10.1021/acs.jpclett.5c02877.
19. Holt RS, Rybolt TR. Modeling enhanced adsorption of explosive molecules on a hydroxylated graphene pore. *Graphene*. 2019;8(1):1-18. doi:10.4236/graphene.2019.81001.
20. Xu S, Zhan J, Man B, Jiang S, Yue W, Gao S, et al. Real-time reliable determination of binding kinetics of DNA hybridization using a multi-channel graphene biosensor. *Nat Commun*. 2017;8(1):14902. doi:10.1038/ncomms14902.
21. Mukherjee S, Bhattacharyya S, Ghosh K, Pal S, Halder A, Naseri M, et al. Sensory development for heavy metal detection: a review on translation from conventional analysis to field-portable sensor. *Trends Food Sci Technol*. 2021;109:674-689. doi:10.1016/j.tifs.2021.01.062
22. Adaryan S, Porter EB, Ardebili H, Verduzco R. Organic electrochemical transistors with molecularly imprinted polymer electrodes for rapid detection of perfluorooctanoic acid. *ACS Appl Mater Interfaces*. 2025;17(17):25582-25590. doi:10.1021/acsami.5c03362.
23. Zanotti R, Berto M, Sensi M, Paradisi A, Veronese E, Pasquato L, et al. Fluorophobic effect enables selective detection of PFAS in water with electrolyte-gated organic transistors. *Adv Funct Mater*. 2025;35(52):Article e202508425. doi:10.1002/adfm.202508425.
24. Kumar A, Kumar A, Kumari S, Singhal NK, Marrazza G, Kumar S. Recent advances and future outlooks towards engineered materials and interfaces for PFAS sensing. *Biosens Bioelectron X*. 2025;27:100706. doi:10.1016/j.biosx.2025.100706.
25. LeBarron CT, Pavithra P, Hosseini S. Recent insights into electrochemical sensing of per- and polyfluoroalkyl substances. *ECS Sens Plus*. 2025;4(3):033601. doi:10.1149/2754-2726/ade79d.
26. Zhang C, Yang Z, Zhu Y, Tan X, Gunjal SJJ, Wang Y, et al. Turning waste into wealth: an efficient platform for capturing, recycling and reusing perfluorinated compounds. *Research Square*. 2023. doi:10.21203/rs.3.rs-3607575/v1.
27. Santiago AR, Dutta A, Wu J, Song Y, Lee YW, Hou C, et al. Investigating the structure-function relationships of fluorinated interfaces for PFAS capture and electrochemically-mediated release. *Adv Funct Mater*. 2025;35(36):Article e202502317. doi:10.1002/adfm.202502317.
28. Tiburtini GA, Bertarini L, Bersani M, Dragani TA, Rolando B, Binello A, et al. In silico prediction of the interaction of legacy and novel per- and poly-fluoroalkyl substances (PFAS) with selected human transporters and of their possible accumulation in the human body. *Arch Toxicol*. 2024;98(9):3035-3047. doi:10.1007/s00204-024-03797-0.

29. Wang S, Ma L, Feng X, Zhang K, Chen Z, Hu M, et al. Portable and cost-effective detection of perfluorooctanesulfonate in water using a screen-printed electrode modified with molecularly imprinted polymer. *ACS ES&T Water*. 2025;5(3):1261-1269. doi:10.1021/acsestwater.4c01044.
30. Çetinkaya A, Yusufbeyoğlu S, Kaya SI, Baldemir A, Atıcı EB, Özkan SA. Plant-based zinc nanoflowers assisted molecularly imprinted polymer for the design of an electrochemical sensor for selective determination of abrocitinib. *Microchim Acta*. 2024;191(6):Article 252. doi:10.1007/s00604-024-06404-2.
31. Jelvehzadeh M, Ghanbari Kh, Zahedi-Tabrizi M. Molecularly imprinted electrochemical sensor based on copper 4-amino benzoic acid metal-organic framework for determination of pregabalin: electrochemical and DFT studies. *Sci Rep*. 2025;15(1):Article number pending. doi:10.1038/s41598-025-19097-1.
32. Arumugam B, Palanisamy S, Janagaraj G, Ramaraj SK, Chiesa M, Subramanian C. Real-time detection of 2,4,6-trichlorophenol in environmental samples using Fe3O4 nanospheres decorated graphitic carbon nitride nanosheets. *Surf Interfaces*. 2023;39:102930. doi:10.1016/j.surfin.2023.102930.
33. Jebril S, Fredj Z, Saeed AA, Gonçalves A, Kaur M, Kumar A, et al. Nanomaterial-based electrochemical chemo(bio)sensors for the detection of nanoplastic residues: trends and future prospects. *RSC Sustain*. 2024;2(4):832-851. doi:10.1039/D3SU00471F.
34. Zhang L, Gionfriddo E, Acquaro VR, Pawliszyn J. Direct immersion solid-phase microextraction analysis of multi-class contaminants in edible seaweeds by gas chromatography-mass spectrometry. *Anal Chim Acta*. 2018;1031:83-97. doi:10.1016/j.aca.2018.05.066.
35. Clark RB, Dick JE. Electrochemical sensing of perfluorooctanesulfonate (PFOS) using ambient oxygen in river water. *ACS Sens*. 2020;5(11):3591-3598. doi:10.1021/acssensors.0c01894.
36. Geng Y, Peveler WJ, Rotello VM. Array-based "chemical nose" sensing in diagnostics and drug discovery. *Angew Chem Int Ed*. 2019;58(16):5190-5200. doi:10.1002/anie.201809607.
37. Shaban SM, Kim D. Recent advances in aptamer sensors. *Sensors (Basel)*. 2021;21(3):979. doi:10.3390/s21030979.
38. Fallah A, Havaei SA, Sedighian H, Kachuei R, Fooladi AAI. Prediction of aptamer affinity using an artificial intelligence approach. *J Mater Chem B*. 2024;12(36):8825-8842. doi:10.1039/D4TB00909F.
39. Xu J, Qiu X, Hildebrandt N. When nanoworlds collide: implementing DNA amplification, nanoparticles, molecules, and FRET into a single microRNA biosensor. *Nano Lett*. 2021;21(11):4802-4808. doi:10.1021/acs.nanolett.1c01351.
40. Bialy RM, Mainguy A, Li Y, Brennan JD. Functional nucleic acid biosensors utilizing rolling circle amplification. *Chem Soc Rev*. 2022;51(21):9009-9067. doi:10.1039/D2CS00613H.
41. Park J, Kim D, Kim DY, Jung J, Zoh K, Lee C, et al. Development of an aptamer-based qPCR method for the selective and rapid picomolar-level detection of perfluorooctanesulfonic acid in water. *Environ Sci Technol*. 2025;59(32):17247-17257. doi:10.1021/acs.est.5c04730.
42. Khadka M, Pasternak YM, Sheinenzon O, Snezhko A, Ronen A, Amiram M, et al. Detection of perfluorooctane sulphonic acid in groundwater using an intelligent array of electrochemical sensors. *J Hazard Mater*. 2025;495:138844. doi:10.1016/j.jhazmat.2025.138844.
43. Moon J, Liu C. Asymmetric CRISPR enabling cascade signal amplification for nucleic acid detection by competitive crRNA. *Nat Commun*. 2023;14(1):Article 7561. doi:10.1038/s41467-023-43389-7.
44. Flores-Contreras EA, González-González RB, Gonzalez-González E, Melchor-Martínez EM, Parra-Saldívar R, Iqbal HMN. Detection of emerging pollutants using aptamer-based biosensors: recent advances, challenges, and outlook. *Biosensors (Basel)*. 2022;12(12):1078. doi:10.3390/bios12121078.
45. Boukherroub R, Szunerits S. The future of nanotechnology-driven electrochemical and electrical point-of-care devices and diagnostic tests. *Annu Rev Anal Chem*. 2024;17(1):173-195. doi:10.1146/annurev-anchem-061622-012029.
46. Kadam US, Cho Y, Park TY, Hong JC. Aptamer-based CRISPR-Cas powered diagnostics of diverse biomarkers and small molecule targets. *Appl Biol Chem*. 2023;66(1):Article 14. doi:10.1186/s13765-023-00771-9.
47. Zhou J, Zhou S, Fan P, Li X, Ying Y, Ping J, et al. Implantable electrochemical microsensors for in vivo monitoring of

animal physiological information. *Nano Micro Lett*. 2024;16(1):Article 28. doi:10.1007/s40820-023-01274-4.
48. Zeppuhar AN, Rollins DS, Huber DL, Bazan-Bergamino EA, Chen F, Evans HA, et al. Linkage transformations in a three-dimensional covalent organic framework for high-capacity adsorption of perfluoroalkyl substances. *ACS Appl Mater Interfaces*. 2023;15(48):56874-56883. doi:10.1021/acsami.3c12826.
49. García L, García-Atienza P, Armenta S, Herrero-Martínez JM, Prejanò M, Marino T, et al. Decoding host-guest interactions: tuning pore functionality in MOFs for efficient capture of short- and long-chain PFAS. *J Mater Chem A*. 2025;13(48):42204-42214. doi:10.1039/D5TA07539D.
50. Zheng X, Li C, Yang N, Niu L, Gao F, Wang Q. Electrochemical sensing of perfluorooctanoic acid via a rationally designed fluorine-functionalized Cu-MOF and in-depth analysis of sensing mechanism. *Anal Chem*. 2025;97(11):6347-6358. doi:10.1021/acs.analchem.5c00745.
51. Wang H, Cao H, Lan W, Zheng H, Cao J, Li Q, et al. Defect-engineered MXene/polypyrrole-TiN hybrid enables ultrasensitive molecularly imprinted electrochemical sensor for highly selective detection of PFOS. *Langmuir*. 2025;41(45):30196-30208. doi:10.1021/acs.langmuir.5c03619.
52. Gavran A, Uskoković-Marković S, Vasiljević BN, Ležaić AJ, Gavrilov N, Milojević-Rakić M, et al. Tracking PFAS using nanomaterial-based sensors: limitations, advances, and challenges. *Chemosensors*. 2025;13(12):421. doi:10.3390/chemosensors13120421.
53. He X. Fundamental perspectives on the electrochemical water applications of metal-organic frameworks. *Nano Micro Lett*. 2023;15(1):Article 148. doi:10.1007/s40820-023-01124-3.
54. Gan L, Wei D, Hu M, Wang Y, Zhou M. Advances in functionalized metal-organic frameworks for PFAS detection: design, mechanisms, performance, and future perspectives. *Small*. 2026;22(5):Article e202509977. doi:10.1002/smll.202509977.
55. Zarei A, Khosropour AR, Khazdooz L, Amirjalayer S, Khojastegi A, Zadehnazari A, et al. Substitution and orientation effects on the crystallinity and PFAS adsorption of olefin-linked 2D COFs. *ACS Appl Mater Interfaces*. 2024;16(7):9483-9494. doi:10.1021/acsami.3c17188.
56. Meng Y, Huang Y, Huang G, Song Y. TPN-COF@Fe-MIL-100 composite used as an electrochemical aptasensor for detection of trace tetracycline residues. *RSC Adv*. 2023;13(40):28148-28157. doi:10.1039/D3RA05452G.
57. Hoque MA, Sommerfeld T, Lisec J, Das P, Prinz C, Heinekamp C, et al. Mechanochemically synthesized covalent organic framework effectively captures PFAS contaminants. *Small*. 2025;21(44):e202509275. doi:10.1002/smll.202509275.
58. Tang H, Qiu L, He L, Zhao L, Qin R, Nan X, et al. Self-assembled stable magnetic COF super-particles through electrostatic interaction for efficient removal and detection of PFAS combined with LC-MS/MS. *Adv Funct Mater*. 2026;36(2):e202512313. doi:10.1002/adfm.202512313.
59. Chakraborty A, Tromer RM, Yadav TP, Mukhopadhyay NK, Lahiri B, Rao R, et al. Ultrasensitive electrochemical sensor for perfluorooctanoic acid detection using two-dimensional aluminium quasicrystal. *arXiv*. 2025:2501.07587. Available from: http://arxiv.org/abs/2501.07587.
60. Özgür C. The analytic hierarchy process method to design applicable decision making for the effective removal of 2-MIB and geosmin in water sources. *Environ Sci Pollut Res Int*. 2024;31(8):12431-12445. doi:10.1007/s11356-024-31848-7.
61. Ogedey A, Oğuz E. Simultaneous removal of COD, NH3-N, and turbidity from sanitary landfill leachate using CB-PAC particles: isotherm modelling and treatment assessment. *Research Square*. 2024. doi:10.21203/rs.3.rs-3906196/v1.
62. Clark RB, Wagner DC, Holden DT, Roberts JJP, Zumbro E, Goodnight L, et al. PFAS electroanalysis in low-oxygen river water using electrogenerated dioxygen. *Environ Sci Technol*. 2023;57(51):21815-21822. doi:10.1021/acs.est.3c03967.
63. Yang Y, Zhang Q, Jin X, Chau CV, Yang J, Henkelman G, et al. Readily visualized perfluorooctanoic acid detection using a small molecule chemosensor. *Angew Chem Int Ed*. 2025;64(19):e202501245. doi:10.1002/anie.202501245.
64. Lu X, Zhong D, An Q, Kang L, Fan N, Cao J, et al. Multiplex nanopore detection of structurally diverse per- and polyfluoroalkyl substances in surface

water. *ACS Nano*. 2025;19(42):37281-37295. doi:10.1021/acsnano.5c12164.
65. Zhao Z, Tian Z, Yan F. Flexible organic electrochemical transistors for bioelectronics. *Cell Rep Phys Sci*. 2023;4(11):101673. doi:10.1016/j.xcrp.2023.101673.
66. Lu Z, Xu K, Xiao K, Xu Q, Wang L, Li P, et al. Biomolecule sensors based on organic electrochemical transistors. *npj Flex Electron*. 2025;9(1):Article number pending. doi:10.1038/s41528-025-00383-x.
67. Reaño RL, Escobar EC. A review of antibody, aptamer, and nanomaterials synergistic systems for an amplified electrochemical signal. *Front Bioeng Biotechnol*. 2024;12:1361469. doi:10.3389/fbioe.2024.1361469.
68. Behrent A, Borggraefe V, Baeumner AJ. Laser-induced graphene trending in biosensors: understanding electrode shelf-life of this highly porous material. *Anal Bioanal Chem*. 2024;416(9):2097-2106. doi:10.1007/s00216-023-05082-y.
69. Grunfeld DA, Gilbert D, Hou J, Jones AM, Lee MJ, Kibbey TCG, et al. Underestimated burden of per- and polyfluoroalkyl substances in global surface waters and groundwaters. *Nat Geosci*. 2024;17(4):340-346. doi:10.1038/s41561-024-01402-8.
70. Dunn M, Bečanová J, Vojta Š, Pickard HM, Lohmann R. Perfluorinated carbon chain length drives uptake of diverse per- and polyfluoroalkyl substances in field-deployed passive samplers. *ACS ES&T Water*. 2025;5(4):1803-1813. doi:10.1021/acsestwater.4c01164.
71. John J, Coulon F, Chellam PV. Detection and treatment strategies of per- and polyfluoroalkyl substances (PFAS): fate of PFAS through DPSIR framework analysis. *J Water Process Eng*. 2022;45:102463. doi:10.1016/j.jwpe.2021.102463.
72. Fagan-Murphy A, Seymour I, Rohan JF, O'Riordan A, O'Connell I. Portable data acquisition system for nano and ultra-micro scale electrochemical sensors. *IEEE Sens J*. 2021;21(3):3072-3080. doi:10.1109/JSEN.2020.3021941.
73. Tang C, Liang Y, Wang K, Liao J, Zeng Y, Luo X, et al. Comprehensive characterization of per- and polyfluoroalkyl substances in wastewater by liquid chromatography-mass spectrometry and screening algorithms. *npj Clean Water*. 2023;6(1):15. doi:10.1038/s41545-023-00220-6.
74. Dong J, Kim S, Young SD, Li C, Jin Z, Lee D, et al. Machine learning for monitoring per- and polyfluoroalkyl substance (PFAS) in California's wastewater treatment plants: an assessment of occurrence and fate. *J Hazard Mater*. 2025;492:138090. doi:10.1016/j.jhazmat.2025.138090.
75. Holton E, Kasprzyk-Hordern B. Multiresidue antibiotic-metabolite quantification method using ultra-performance liquid chromatography coupled with tandem mass spectrometry for environmental and public exposure estimation. *Anal Bioanal Chem*. 2021;413(23):5901-5920. doi:10.1007/s00216-021-03573-4.
76. Weidemann E, Lämmer R, Stahl T, Göckener B, Bücking M, Breuer J, et al. Leaching and transformation of perfluoroalkyl acids and polyfluoroalkyl phosphate diesters in unsaturated soil column studies. *Environ Toxicol Chem*. 2022;41(9):2065-2077. doi:10.1002/etc.5417.
77. Louisse J, Rijkers D, Stoopen G, Janssen AWF, Staats M, Hoogenboom LAP, et al. Perfluorooctanoic acid (PFOA), perfluorooctane sulfonic acid (PFOS), and perfluorononanoic acid (PFNA) increase triglyceride levels and decrease cholesterogenic gene expression in human HepaRG liver cells. *Arch Toxicol*. 2020;94(9):3137-3155. doi:10.1007/s00204-020-02808-0.
78. Fenton SE, Ducatman A, Boobis AR, DeWitt JC, Lau C, Ng CA, et al. Per- and polyfluoroalkyl substance toxicity and human health review: current state of knowledge and strategies for informing future research. *Environ Toxicol Chem*. 2021;40(3):606-630. doi:10.1002/etc.4890.
79. Tabar FA, Lowdon JW, Sichani SB, Khorshid M, Cleij TJ, Diliën H, et al. An overview on recent advances in biomimetic sensors for the detection of perfluoroalkyl substances. *Sensors (Basel)*. 2024;24(1):130. doi:10.3390/s24010130.
80. Laghlimi C, Moutcine A, Chtaini A, Isaad J, Soufi A, Ziat Y, et al. Recent advances in electrochemical sensors and biosensors for monitoring drugs and metabolites in pharmaceutical and biological samples. *ADMET DMPK*. 2023;11(3):327-356. doi:10.5599/admet.1709.
81. Li S, Zhang H, Zhu M, Kuang Z, Li X, Xu F, et al. Electrochemical biosensors for whole blood analysis: recent progress,

challenges, and future perspectives. *Chem Rev*. 2023;123(12):7953-8039. doi:10.1021/acs.chemrev.1c00759.
82. Matteo PD, Petrucci R, Curulli A. Not only graphene two-dimensional nanomaterials: recent trends in electrochemical (bio)sensing area for biomedical and healthcare applications. *Molecules*. 2024;29(1):172. doi:10.3390/molecules29010172.
83. Lorencová L, Kasák P, Košútová N, Jerigová M, Noskovičová E, Vikartovská A, et al. MXene-based electrochemical devices applied for healthcare applications. *Microchim Acta*. 2024;191(2):79. doi:10.1007/s00604-023-06163-6.
84. Liu H, Wang Z, Zhou G. Wearable sensors for monitoring workplace chemical exposures in occupational health management. *Anal Methods*. 2025;17(39):7863-7889. doi:10.1039/D5AY00961H.
85. Liu H, Song J, Zhao Z, Zhao S, Tian Z, Yan F. Organic electrochemical transistors for biomarker detections. *Adv Sci (Weinh)*. 2024;11(27):2305347. doi:10.1002/advs.202305347.
86. Khan R, Uygun ZO, Andreescu D, Andreescu S. Sensitive detection of perfluoroalkyl substances using MXene-AgNP-based electrochemical sensors. *ACS Sens*. 2024;9(6):3403-3412. doi:10.1021/acssensors.4c00776.
87. Frigerio G, Cafagna S, Polledri E, Mercadante R, Fustinoni S. Development and validation of an LC-MS/MS method for the quantitation of 30 legacy and emerging per- and polyfluoroalkyl substances (PFASs) in human plasma, including HFPO-DA, DONA, and cC6O4. *Anal Bioanal Chem*. 2022;414(3):1259-1278. doi:10.1007/s00216-021-03762-1.
88. Zhang H, Li Y, Abdallah MF, Tan H, Li J, Liu S, et al. Novel one-point calibration strategy for high-throughput quantitation of microcystins in freshwater using LC-MS/MS. *Sci Total Environ*. 2023;858:159345. doi:10.1016/j.scitotenv.2022.159345.
89. Antonacci A, Scognamiglio V, Mazzaracchio V, Caratelli V, Fiore LD, Moscone D, et al. Paper-based electrochemical devices for the pharmaceutical field: state of the art and perspectives. *Front Bioeng Biotechnol*. 2020;8:339. doi:10.3389/fbioe.2020.00339.
90. Furlong ET, Noriega MC, Kanagy CJ, Kanagy LK, Coffey LJ, Burkhardt MR. Determination of human-use pharmaceuticals in filtered water by direct aqueous injection: high-performance liquid chromatography/tandem mass spectrometry. *Tech Methods*. 2014;5-B10. doi:10.3133/tm5b10.
91. Bartelt-Hunt SL, Snow DD, Damon T, Shockley J, Hoagland KD. The occurrence of illicit and therapeutic pharmaceuticals in wastewater effluent and surface waters in Nebraska. *Environ Pollut*. 2009;157(3):786-791. doi:10.1016/j.envpol.2008.11.025.
92. Newman S, Wilson BD, Mamerow D, Wollant BC, Nyein HYY, Rosenberg-Hasson Y, et al. Extending the dynamic range of biomarker quantification through molecular equalization. *Nat Commun*. 2023;14(1):Article 4298. doi:10.1038/s41467-023-39772-z.
93. Fauskanger PK, Sandberg S, Johansen JV, Keller T, Budd JR, Miller WG, et al. Quantification of difference in nonselectivity between in vitro diagnostic medical devices. *Biometrical J*. 2025;67(1):e70032. doi:10.1002/bimj.70032.
94. Cogorno J, Rolle M. Impact of variable water chemistry on PFOS-goethite interactions: experimental evidence and surface complexation modeling. *Environ Sci Technol*. 2024;58(3):1731-1740. doi:10.1021/acs.est.3c09501.
95. Navarathna C, Boateng RA, Luo L. Challenges in PFAS postdegradation analysis: insights from the PFAS-CTAB model system. *ACS Meas Sci Au*. 2025;5(1):135-144. doi:10.1021/acsmeasuresciau.4c00083.
96. Liang WS, Beaulieu-Jones BK, Smalley SL, Snyder M, Goetz LH, Schork NJ. Emerging therapeutic drug monitoring technologies: considerations and opportunities in precision medicine. *Front Pharmacol*. 2024;15:1348112. doi:10.3389/fphar.2024.1348112.
97. Medina H, Farmer C. Current challenges in monitoring low contaminant levels of per- and polyfluoroalkyl substances in water matrices in the field. *Toxics*. 2024;12(8):610. doi:10.3390/toxics12080610.
98. Amin N, Chen J, Nguyen NT, He Q, Schwartz JS, Wu J. Rapid and ultrasensitive sensor for point-of-use detection of perfluorooctanoic acid based on molecular imprinted polymer and AC electrothermal effect. *Micromachines (Basel)*. 2025;16(3):283. doi:10.3390/mi16030283.

99. Elnakar H. Automated machine learning and SHAP-based interpretation of PFOA removal via electrochemical oxidation. *Desalin Water Treat*. 2025;325:101598. doi:10.1016/j.dwt.2025.101598.
100. Maity A, Pu H, Sui X, Chang J, Bottum KJ, Jin B, et al. Scalable graphene sensor array for real-time toxins monitoring in flowing water. *Nat Commun*. 2023;14(1):Article 4264. doi:10.1038/s41467-023-39701-0.
101. Li R, Gibson JM. Predicting the occurrence of short-chain PFAS in groundwater using machine-learned Bayesian networks. *Front Environ Sci*. 2022;10:958784. doi:10.3389/fenvs.2022.958784.
102. A 'Wikipedia for cells': researchers get an updated look at the Human Cell Atlas, and it's remarkable. *Nature*. 2024;635(8039):523-524. doi:10.1038/d41586-024-03754-y.
103. Sim JK, Brothers M, Slocik JM, Islam AE, Maruyama B, Grigsby CC, et al. Biomarkers and detection platforms for human health and performance monitoring: a review. *Adv Sci (Weinh)*. 2022;9(7):2104426. doi:10.1002/advs.202104426.
104. Sahu SP, Kole S, Arges CG, Gartia MR. Rapid and direct perfluorooctanoic acid sensing with selective ionomer coatings on screen-printed electrodes under environmentally relevant concentrations. *ACS Omega*. 2022;7(6):5001-5007. doi:10.1021/acsomega.1c05847.
105. Nalakurthi NVSR, Abimbola I, Ahmed T, Anton I, Riaz K, Ibrahim Q, et al. Challenges and opportunities in calibrating low-cost environmental sensors. *Sensors (Basel)*. 2024;24(11):3650. doi:10.3390/s24113650.
106. Sahu NP, Maldhure AV. Framework for evaluating the performance of water quality sensors. *Cleaner Water*. 2025;4:100144. doi:10.1016/j.clwat.2025.100144.
107. Ali H, Khilji M, Buledi JA, Memon AA, Ghanghro AB, Rehman M ur, et al. MXene-based nanocomposites: a new horizon for electrochemical monitoring of environmental pollutants. *RSC Sustain*. 2025;3(5):2160-2184. doi:10.1039/D4SU00828F.
108. Bounegru AV, Dinu A, Iticescu C, Georgescu L. Electrochemical sensors and biosensors for the detection of pharmaceutical contaminants in natural waters—a comprehensive review. *Chemosensors*. 2025;13(2):65. doi:10.3390/chemosensors13020065.